P67-phox-Mediated NADPH Oxidase Assembly: Imaging of Cytochrome b_{558} Liposomes by Atomic Force Microscopy†

Marie-Hélène Paclet,‡ Anthony W. Coleman,§ Sabrina Vergnaud,‡ and Françoise Morel*,‡

GREPI EA 2938 MENRT laboratoire Enzymologie, CHU Grenoble BP 217, 38043 Grenoble Cedex, France, and IBCP CNRS UPR 412, 7 passage de Vercors, 69367 Lyon Cedex, France

Received March 2, 2000; Revised Manuscript Received May 1, 2000

ABSTRACT: NADPH oxidase activity depends on the assembly of the cytosolic activating factors, p67-phox, p47-phox, p40-phox, and Rac with cytochrome b_{558}. The transition from an inactive to an active oxidase complex induces the transfer of electrons from NADPH to oxygen through cytochrome b_{558}. The assembly of oxidase complex was studied in vitro after reconstitution in a heterologous cell-free assay by using true noncontact mode atomic force microscopy. Cytochrome b_{558} was purified from neutrophils and Epstein−Barr virus-immortalized B lymphocytes and incorporated into liposomes. The effect of protein glycosylation on liposome size and oxidase activity was investigated. The liposomes containing the native hemoprotein purified from neutrophils had a diameter of 146 nm, whereas after deglycosylation, the diameter was reduced to 68 nm, although oxidase activity was similar in both cases. Native cytochrome b_{558} was used after purification in reconstitution experiments to investigate the topography of NADPH oxidase once it was assembled. For the first time, atomic force microscopy illustrated conformational changes of cytochrome b_{558} during the transition from the inactive to the active state of oxidase; height measurements allow the determination of a size of 4 nm for the assembled complex. In the processes that were studied, p67-phox displayed a critical function; it was shown to be involved in both assembly and activation of oxidase complex while p47-phox proceeded as a positive effector and increased the affinity of p67-phox with cytochrome b_{558}, and p40-phox stabilizes the resting state. The results suggest that although an oligomeric structure of oxidase machinery has not been demonstrated, allosteric regulation mechanisms may be proposed.

Cytochrome b_{558} of the NADPH oxidase complex generates superoxide anion O_2^- in phagocytic cells and B lymphocytes through a membrane-spanning electron transport chain from NADPH to molecular oxygen (*1*, *2*). It is a heme-containing integral membrane protein consisting of two α- and β-subunits, p22-phox and gp91-phox with a stoichiometry of 1/1 (*3*); gp91-phox is heavily glycosylated (*4*−*6*) while p22-phox is not, and it has been proposed as the sole heme-binding subunit of cytochrome b_{558} (*7*). Coexpression of gp91-phox and p22-phox is required to support O_2^- production (*8*), but oxidase activity depends on the assembly of three cytosolic activating factors, p47-phox, p67-phox, and p40-phox, and a small G protein Rac1- or -2 with cytochrome b_{558} at the membrane level (*9*−*13*).

The exact mechanism of oxidase activation still remains unclear. Phosphorylation of p47-phox following ligand receptor interaction in intact cells and arachidonic acid stimulation in a cell-free assay probably initiate translocation and assembly (*14*). The assembly process involves a cascade of multiple protein−protein interactions between the various oxidase components.

In the cytosol of resting cells, p67-phox and p40-phox associate (*15*). Cell stimulation induces the conformational change of p47-phox followed by the translocation of the p67-phox−p40-phox−p47-phox complex to the membrane environment. After dissociation from rho-GDI in cytosol, Rac migrates to the membrane; after binding via its geranylgeranyl tail and exchange of GDP over GTP, the active GTP-bound Rac potentiates oxidase activity (*10*). A direct interaction of Rac-GTP with the N-terminal domain of p67-phox has been demonstrated (*16*), and moreover, very recently, GTP-bound Rac was reported to be involved in the dissociation of the p67-phox−p40-phox complex during activation (*17*). While the p40-phox function remains obscure, it has been shown to decrease NADPH oxidase activity (*11*, *15*). Recent data from in vitro experiments pointed to p67-phox as the essential factor of NADPH oxidase activation (*18*, *19*), and gp91-phox has been proposed to be the component responsible for the electron transfer from NADPH to oxygen (*7*).

A heterologous cell-free assay (*20*) was used to study in vitro the assembly process, in which purified cytochrome b_{558} from neutrophils or from Epstein−Barr virus B lymphocytes incorporated into liposomes was either incubated

† This work was supported by grants from the "Direction de l'Economie, de la Recherche et de l'Enseignement Supérieur, the Région Rhône Alpes, programme Emergence", the "Faculté de Médecine-Université Joseph Fourier, Grenoble I", and the "Ministère de l'Enseignement Supérieur et de la Recherche", Paris. We acknowledge the financial support of IMABIO (CNRS), MPCV (CNRS), and "la Fondation pour la Recherche Médicale" for the atomic force microscopy.

* Corresponding author. E-mail: FrMorel.enzymo@chu-grenoble.fr. Phone: 33 (0)4 76 76 54 83. Fax: 33 (0)4 76 76 56 08.

‡ GREPI EA 2938 MENRT.

§ IBCP CNRS UPR 412.

10.1021/bi000483j CCC: $19.00
Published on Web 07/13/2000

with the cytosolic factors in cytosol or isolated from it or as recombinant proteins. The transition from the inactive to the active oxidase complex was mediated by arachidonic acid (*20*).

The incorporation of membrane proteins into liposomes preserves the lipophilic bilayer environment by which such proteins are anchored to cell walls (*21*), and as a consequence, the activity of the proteins is normally conserved. The cell wall structure is complex; the use of the liposome−protein systems allows single effects (such as protein glycosylation and ionic activation) to be identified and studied in detail (*22*). Also, as the protein activity is conserved, the assembly of supramolecular multiprotein complexes may also be observed and their activity investigated. Atomic force microscopy (AFM)[1] allows the observation of untreated surface structures in air or under solutions and as a consequence of particular interest for soft and active systems such as biological assemblies. Atomic force microscopy is one of a class of techniques in which interaction between a local probe and a surface is used, by means of scanning close to the surface, to generate very high resolution on the nature of the substrate. While a wide range of information may be obtained, including chemical nature, electrical properties, and electronic and magnetic properties, the technique is most widely used with biological samples to provide topographic imaging of the surface of the substrate by simple measurement of the deflection of a laser beam reflected from a cantilever at the base of which a tip is held at a constant distance from the sample during scanning (*23*). Three basic scanning modes exist for atomic force microscopy. The first is the contact mode in which the feedback loop is established with the AFM tip in van der Waals contact with the surface; this provides high-resolution topographic imaging, but the large forces that are applied can cause lateral distortion or even sample displacement for soft or weakly adhering samples. The true noncontact mode is the second. Here, the tip is oscillated at high frequency, generally in the range of 100−300 kHz, the feedback loop is established in the attractive region, and the tip never contacts the sample. This is best suited to soft samples and in particular to height measurement; however, lateral resolution is reduced to the nanometer range. The third is the tapping mode, in which the feedback loop is established outside van der Waals contact. However, a periodic beat brings the tip into contact with the sample; no lateral forces are applied, but strong tip−sample interactions occur in the *z*-direction. This method yields high-resolution imaging, but sample compression renders it unsuitable for height measurement (*24*). AFM has been widely used for the study of bio-macromolecules (*25*, *26*), supramolecular assembly of biological sytems (*22*), and measurement of interaction forces between receptors and ligands (*27*). However, imaging of proteins incorporated in liposomes (*28*, *29*) is less widely reported, due to liposome fragility and their possibility of spreading, forming bilayers on mica surfaces (*22*). While high-resolution imaging is then possible in such supported bilayers, information about the height and size of complexes formed by membrane proteins cannot be obtained. In this paper, the use of true noncontact mode AFM prevents high-resolution imaging but ensures that the process does not disturb the liposome structure (*24*).

The study presented here investigates the topography of active NADPH oxidase complex using atomic force microscopy through an in vitro cell-free oxidase reconstitution. The findings illustrate for the first time the effect of protein glycosylation on liposome size and focus on conformational changes of the complex related to the transition between the resting and activated states of oxidase and assembly of cytosolic activating factors with cytochrome b_{558}. In this process, p67-phox is the critical component of activation.

MATERIALS AND METHODS

Materials. The following materials were supplied by the indicated companies: diisopropyl fluorophosphate (DFP) (Acros Organics); phorbol myristate acetate (PMA), N^{α}-*p*-tosyl-L-lysine chloromethyl ketone (TLCK), leupeptin (hemisulfate salt, from microbial source), L-α-phosphatidylcholine (type II-S), and heparin−agarose (Sigma Chemicals, St. Louis, MO); sucrose monolaurate, endoglycosidase F/N-glycosidase F (from *Flavobacterium meningosepticum*), phenylmethanesulfonyl fluoride (PMSF), pepstatin, and *n*-octyl glucoside (Roche Diagnostics, Meylan, France); Sephacryl S-300 HR, DEAE Sepharose CL-6B, CM Sepharose CL-6B, and octyl Sepharose CL-4B (Pharmacia LKB, Biotechnology, Uppsala, Sweden); ECL Western blotting detection reagents (Amersham, Buckinghamshire, U.K.); and 2 mg/mL Ciprofloxacine (Ciflox) (Bayer Pharma, Puteaux, France). Monoclonal antibodies mAb48 and mAb449 were a generous gift from D. Roos and A. Verhoeven. The cDNA encoding p47-phox cloned into the plasmid pGEX-2T was a generous gift from A. W. Segal and F. Wientjes.

Lymphoid Cell Line and Neutrophils. Citrate-sterile venous blood was drawn from either healthy patients or a CGD patient with previously characterized CGD AR p67-phox(−) (*30*) after informed consent. Neutrophils and B lymphocytes were isolated by Ficoll-Hypaque density gradient centrifugation (*20*). Lymphocytes were collected at the Ficoll surface and infected with the B95-8 strain of Epstein−Barr virus (EBV) as described previously (*20*). The EBV-B lymphocyte cell lines were kept in culture using RPMI 1640 supplemented with 10% fetal calf serum, 2 mM L-glutamine, and 2 μg/mL Ciflox, at 37 °C under a 5% CO_2 atmosphere. Neutrophils were collected in the pellet after red-cell hypotonic lysis (*30*). Crude membrane and cytosol fractions from both cell types were prepared as reported previously (*20*).

Purification of Cytochrome b_{558} from Neutrophils. Cytochrome b_{558} was purified from the plasma membranes of 10^{10} phorbol ester-stimulated neutrophils as reported previously (*31*). Cytochrome b_{558} was extracted from membrane using 68 mM *n*-octyl glucoside. Prior to relipidation of purified cytochrome b_{558}, Triton X-100 was replaced with 40 mM *n*-octyl glucoside (*31, 32*). Relipidation was performed in the presence of L-α-phosphatidylcholine II-S; 100 μg of phospholipids was mixed with 400 pmol of purified cytochrome b_{558}, and the mixture was briefly sonicated, diluted 6-fold with detergent-free buffer containing 120 mM NaH_2PO_4 (pH 7.2), 1 mM $MgCl_2$, 1 mM dithiothreitol, 20% (v/v)

[1] Abbreviations: AFM, atomic force microscopy; BSA, bovine serum albumin; EBV, Epstein−Barr virus; ECL, enhanced chemiluminescence; EGTA, ethylene glycol bis(β-aminoethyl ether); FAD, flavin adenine dinucleotide; GTPγS, guanosine 5′-*O*-(γ-thiotriphosphate); *n*-octyl glucoside, 1-*O*-*n*-octyl β-D-glucopyranoside; phox, phagocyte oxidase; SDS, sodium dodecyl sulfate; SD, standard deviation.

glycerol, 1 mM EGTA, and the antiprotease mixture (10 μM N^{α}-*p*-tosyl-L-lysine chloromethyl ketone, 1.8 μM leupeptin, 1.5 μM pepstatin, and 1 mM phenylmethanesulfonyl fluoride), and incubated for 30 min on ice (*21*). Liposomes were stored at −80 °C before further use.

Purification of Cytochrome b_{558} from EBV-B Lymphocytes. EBV-B lymphocytes (2×10^{10} cells) were suspended at a concentration of 10^8 cells/mL in PBS supplemented with the previous antiprotease coktail mixture, sonicated for 2×10 s at 40 W using a Branson sonifier, and centrifugated at 1000*g* for 15 min at 4 °C. The postnuclear supernatant was overlaid on a discontinuous sucrose gradient comprising two 4 mL sucrose layers of 35% (w/v) and 15% (w/v). Centrifugation was carried out using a SW 41 rotor at 150000*g* for 75 min. The plasma membrane-enriched fraction located at the interface between the two sucrose layers was collected and diluted 2-fold in PBS containing the antiprotease mixture. After centrifugation at 100000*g* for 45 min at 4 °C, membrane proteins were solubilized with 1% (w/v) sucrose monolaurate (final concentration) for 20 min, incubated at 4 °C, and centrifuged at 200000*g* for 60 min at 4 °C. The solubilized extract was submitted to three chromatographic steps as described above for neutrophil cytochrome b_{558} purification. Cytochrome b_{558} purified from EBV-B lymphocytes was relipidated after detergent exchange as described above.

Preparation of Antibodies against p47-phox. A polypeptide corresponding to the COOH-terminal region of p47-phox (residues 371−390) was synthesized by Neosystem (Strasbourg, France). Antiserum against this KLH-coupled synthetic polypeptide was raised in rabbits by repeated injections and used for Ig purification with 1 mL of a protein A Sepharose CL-4B matrix (*31*).

Isolation of the p47-phox−p67-phox−p40-phox Complex. Anti-p47-phox Igs were immobilized on Carbolink coupling gel through their oxidized carbohydrate moiety according to the manufacturer's instructions. Cytosol from EBV-B lymphocytes (50−100 mg of protein, i.e., $2-5 \times 10^9$ cell equivalents) of either a healthy or a p67-phox-deficient CGD patient p67-phox(−) was added on the Carbolink matrix equilibrated in PBS with overnight recycling at 4 °C. After being washed in PBS, the bound proteins were eluted with 0.1 M glycine at pH 2.5. Eluates were immediately buffered with 1 M Tris-HCl (pH 9.5) and then pooled and dialyzed against PBS.

Recombinant Proteins. Full-length cDNAs encoding p40-phox, p67-phox, p47-phox, and Rac1 were expressed in *Escherichia coli* as a glutathione *S*-transferase (GST) fusion protein using pGEX-5X-2, pGEX-3X, and pGEX-2T, respectively (*32*, *33*). Protein expression was induced with isopropyl thiogalactoside (0.2 mM for p67-phox and 0.1 mM for p40-phox and Rac1) at 37 °C (or at 20−26 °C for p67-phox). The p67-phox and Rac1 fusion proteins were affinity purified from IPTG-induced bacteria on glutathione−Sepharose followed by Xa factor and thrombin cleavage, respectively (the protein Rac1 was cleaved directly on the affinity column) (*32*). During the preparation of rp40-phox, a small fraction was solubilized, but the major part was collected as inclusion bodies; 1% Triton X-100 and then 8 M urea were used for extraction (*15*). The rp40-phox−GST fusion protein was purified on the glutathione−Sepharose 4B affinity matrix before further use.

Deglycosylation Experiments. Purified cytochrome b_{558} from neutrophils (36 pmol) was denatured after relipidation by heating at 100 °C for 2 min in the presence of 0.2% (w/v) SDS and 1% (w/v) β-mercaptoethanol. At the end of the incubation, 34 mM *n*-octyl glucoside and then 0.2 unit of endoglycosidase F/N-glycosidase F were added for incubation for a further 4 h at 37 °C. The reaction was stopped by cooling to 4 °C. Then, 6 pmol of native or deglycosylated cytochrome b_{558} liposomes from neutrophils were subjected to 10% SDS−PAGE followed by Western blotting (*34*). For the reconstituted oxidase activity experiments, deglycosylation was performed without detergent and β-mercaptoethanol, and 12 pmol of purified cytochrome b_{558} from neutrophils were incubated for 8 h at 37 °C with 0.2 unit of endoglycosidase F/N-glycosidase F.

Reconstitution of Oxidase Activity. In vitro reconstitution of an active oxidase complex was mediated in a cell-free assay by incubating 2×10^{-3} μM purified native or deglycosylated cytochrome b_{558} from neutrophils or EBV-B lymphocytes inserted into liposomes with 300 μg of neutrophil cytosol obtained from resting cells or EBV-B lymphocyte cytosol of healthy or p67-phox-deficient CGD patients. The medium for oxidase reconstitution contained 40 μM GTPγS, 5 mM $MgCl_2$, and an optimum amount of arachidonic acid (40−100 nmol) in a final volume of 100 μL (*20*). In certain experiments, the cytosol was replaced with the p47-phox−p67-phox−p40-phox complex (10 μg of proteins) isolated from EBV-B lymphocyte cytosol onto the Carbolink affinity matrix or with the purified recombinant proteins: rRac1 (0−1 μM), rp67-phox (0−2 μM), rp47-phox (0.17 μM), and rp40-phox−GST (0−0.3 μM). Under the latter conditions, the reconstitution medium was complemented with 10 μM FAD. After incubation for 10 min at 25 °C, it was transferred to a photometric cuvette for measurement of the rate of superoxide anion formation. Reconstituted oxidase activity was assessed by measuring the superoxide dismutase-sensitive portion of ferricytochrome *c* reduction (*20*) recorded at 550 nm ($\Sigma_{550} = 21.1$ mM^{-1} cm^{-1}).

Gel Electrophoresis. SDS−PAGE was carried out using 10% polyacrylamide resolving gels containing 0.2% (w/v) SDS and a 5% stacking gel (*35*). Proteins were detected by staining with silver nitrate (*36*).

Immunoblotting. Purified cytochrome b_{558} was submitted to 10% SDS−PAGE, and it was electrotransferred from acrylamide to nitrocellulose at 30 mA for 75 min (*37*). Nitrocellulose was incubated for 1 h in 0.05% (w/v) TBS-Tween containing 3% (w/v) BSA and then with monoclonal antibody mAb48 (1/500) or mAb449 (1/500) directed against the β-subunit or α-subunit, respectively, of neutrophil cytochrome b_{558}. The immune complexes were detected with goat anti-mouse secondary antibody conjugated to peroxidase. The bound peroxidase activity was detected by using ECL reagents (Amersham Life Science).

AFM Experimentation. Liposomes (5 μL, i.e., 0.1 μg of protein) containing native or deglycosylated cytochrome b_{558} purified from neutrophils were allowed to adhere to a mica surface for 30 s to 1 min. After the sample had been washed three times and dried in air overnight, image observation was performed using true noncontact AFM at room temperature. AFM measurements were carried out in air using a Topometrix Explorer AFM system in the low-amplitude true noncontact mode, using either low-frequency or high-

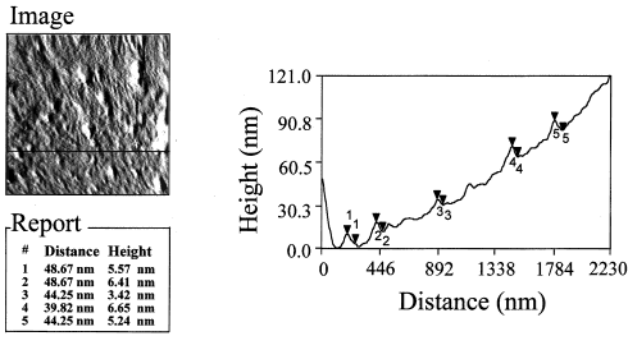

FIGURE 1: Calculation of liposome size. AFM liposome images are represented in the left panel. The right-hand curve illustrates the topography of the left-hand liposome preparation cut (black line). The diameter and height of liposomes were determined by using Topometrix software after calculation of the distance between two selected points on the curve as shown in the right panel.

frequency cantilevers (Silicon SFM probes, Topometrix). Scan rates were between 0.5 and 1 Hz and were set so as to minimize noise. Calculation of liposome size is explained in Figure 1; the diameter and height of liposomes were determined on *x* images of *y* different experiments by using Topometrix software after calculation of the distance between two selected points, representing the edges of the liposomes, on the curve.

For assembly experiments, the medium of reconstituted activity was prepared as described in Reconstitution of Oxidase Activity with 2×10^{-3} μM cytochrome b_{558} purified from neutrophils and incorporated into liposomes and either cytosol prepared from neutrophils or EBV-B lymphocytes (300 μg) or recombinant proteins: rp47-phox (0.17 μM), rp67-phox (0.5 or 1.5 μM), rp40−GST (0.15 μM), and rRac1 (0.1 μM). Aliquot fractions (5−10 μL) were collected from the mixture before and after addition of an optimal amount of arachidonic acid, spread on a mica surface, and allowed to adhere for 30 s to 1 min, followed by three washings and overnight desiccation before observation by AFM. Liposome images from AFM were analyzed using the software SPM Lab 3.06 (Topometrix); the diameter and height were determined from *n* liposome cross sections. Statistical analysis of *n* measurements was carried out; mean values are given. Calculation of liposome size is explained in Figure 1.

RESULTS

Effect of Deglycosylation on NADPH Oxidase Activity, and AFM Structure. Cytochrome b_{558} was purified from neutrophils (PMN) and incorporated into L-α-phosphatidylcholine liposomes as described in Materials and Methods. The efficiency of purification is illustrated by SDS−PAGE and Western blotting in Figure 2 (lane 1, and lanes 2 and 3, respectively). Purified cytochrome b_{558} was deglycosylated by incubation with endoglycosidase F/N-glycosidase F. Oxidase activity of deglycosylated cytochrome b_{558} was controlled by using a cell-free assay (*20*, *32*) and compared to that measured with native cytochrome b_{558}. Oxidase reconstitution was mediated with neutrophil cytosol, GTPγ-[S], FAD, $MgCl_2$, and an optimal amount of arachidonic acid as an amphiphilic activator. There was no significant difference in turnover of reconstituted oxidase as measured with deglycosylated or native cytochrome b_{558}: 79 versus 89 mol of O_2^- s^{-1} (mol of heme *b*)$^{-1}$ (Table 1). The deglycosylated structure of cytochrome b_{558} was confirmed by immunoreaction with monoclonal antibody mAb48 raised against the β-subunit of cytochrome b_{558}, using SDS−PAGE and Western blotting (panels B and C of Figure 3, lanes 1). The immune complexes were detected by luminescence with goat anti-mouse secondary antibody conjugated to peroxidase. The broad diffuse band of 80−91 kDa was transformed into a single band of 55 kDa.

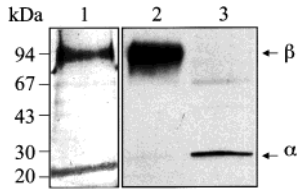

FIGURE 2: SDS−PAGE and Western blot analysis of purified cytochrome b_{558} from human neutrophils. Purified cytochrome b_{558} (100 pmol) was submitted to SDS−PAGE (10%) and silver stained (lane 1). Western blot was performed by ECL with 20 pmol of purified cytochrome b_{558} using monoclonal antibodies raised against the β-subunit (mAb48) (lane 2) or against the α-subunit (mAb449) (lane 3) of cytochrome b_{558} as described in Materials and Methods.

Table 1: Measurement of Cytochrome b_{558} Liposome Size and of Oxidase Activity before and after Deglycosylation[a]

	neutrophil cytochrome b_{558} liposomes		control liposomes	
	native ($n = 18$)	deglycosylated ($n = 13$)	small ($n = 16$)	large ($n = 45$)
diameter (nm)	146 ± 19	68 ± 5	40 ± 3	154 ± 23
height (nm)	5 ± 1	4 ± 1	4 ± 1	13 ± 4
rate of oxidase turnover [mol of O_2^- s^{-1} (mol of heme *b*)$^{-1}$]	89 ± 11	79 ± 6	−	−

[a] Liposomes (5 μL, i.e., 0.1 μg of protein) containing native or deglycosylated cytochrome b_{558} purified from neutrophils were allowed to adhere on a mica surface for 30 s to 1 min. Control liposomes were made with phospholipids suspended in the deglycosylation buffer. After the sample had been washed three times and air-dried overnight, image observation was performed using AFM in the noncontact mode at room temperature. AFM measurements were carried out using a Topometrix Explorer atomic force microscope in the low-amplitude true noncontact mode, using either low-frequency or high-frequency cantilevers. Scan rates were between 0.5 and 1 Hz and were set so as to minimize noise. The results are representative of *n* liposome images ± SD. Reconstituted oxidase activity medium was prepared as described in Materials and Methods, with native or deglycosylated cytochrome b_{558} purified from neutrophils (2×10^{-3} μM) in the presence of neutrophil cytosol (300 μg). In this case, deglycosylation was performed without protein denaturation (see Materials and Methods). Turnover was assessed by the ferricytochrome *c* reduction after addition of an optimal amount of arachidonic acid.

Integration of both native and deglycosylated purified cytochrome b_{558}, obtained from neutrophils, into L-α-phosphatidylcholine liposomes leads to stable structures which have been deposited onto freshly cleaved mica surfaces as intact systems that are suitable for AFM studies (*22*). Three-dimensional AFM images are shown in Figure 3A; the images obtained for the two sets of liposomes are given in panels B and C of Figure 3 (lanes 2). The dimensions are summarized in Table 1 along with the control experiment using liposomes prepared in the presence of the SDS and octyl glucoside detergents, necessary for the deglycosylation procedure, but in the absence of cytochrome b_{558}. The large sample sizes allow accurate statistical analysis.

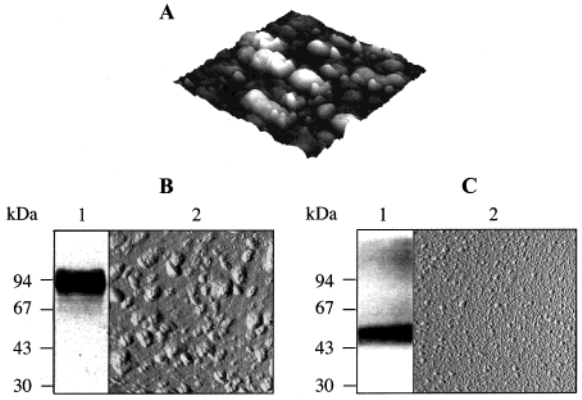

FIGURE 3: Effect of cytochrome b_{558} deglycosylation on liposome topography observed via atomic force microscopy (AFM). Liposomes (5 μL, i.e., 0.1 μg of protein) containing native (A and B, lane 2) or deglycosylated (C, lane 2) cytochrome b_{558} purified from neutrophils were allowed to adhere on a mica surface for 30 s to 1 min. After the sample had been washed three times and air-dried overnight, image observation was performed using AFM in the noncontact mode at room temperature. AFM measurements were carried out using a Topometrix Explorer atomic force microscope in the low-amplitude true noncontact mode, using either low-frequency or high-frequency cantilevers. Scan rates were between 0.5 and 1 Hz, and were set so as to minimize noise. In panel A, a three-dimensional image of liposomes containing native cytochrome b_{558} purified from neutrophils is represented. (B and C) Immunodetection of purified native and deglycosylated cytochrome b_{558}, respectively (lanes 1). N-Linked oligosaccharides of purified cytochrome b_{558} were removed by incubation with 0.2 unit of endoglycosidase F/N-glycosidase F. Before deglycosylation, purified cytochrome b_{558} from neutrophils (36 pmol) was denatured after relipidation as described in Materials and Methods. Native or deglycosylated cytochrome b_{558} liposomes from neutrophils were subjected to 10% SDS−PAGE followed by Western blotting (*37*). After incubation of nitrocellulose with monoclonal antibody 48 (1/500) directed against the β-subunit of neutrophil cytochrome b_{558}, the immune complexes were detected with goat anti-mouse secondary antibody conjugated to peroxidase; bound peroxidase was detected by using ECL reagents.

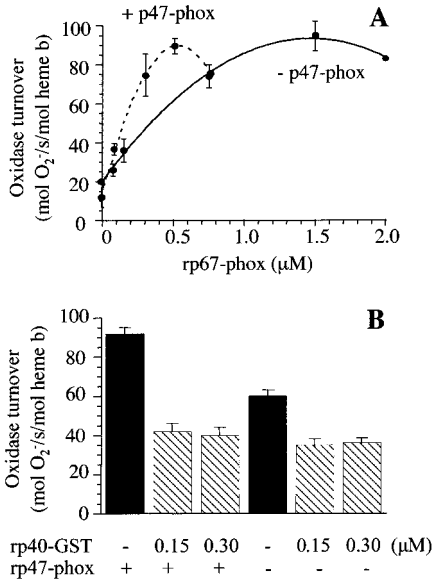

FIGURE 4: Reconstitution of oxidase activity with recombinant cytosolic factors in the presence or absence of p47-phox. (A) Reconstitution experiments were performed as described in Materials and Methods, by using cytochrome b_{558} purified from neutrophils (2×10^{-3} μM), rRac1 (0.1 μM), and an increased amount of rp67-phox (0−2 μM) in the presence (- - -) or absence (—) of rp47-phox (0.17 μM). Turnover values are mean averages (±SD) from at least three assays. (B) Effect of rp40-phox−GST on the reconstituted oxidase turnover. Cell-free activation of NADPH oxidase was performed with cytochrome b_{558} (2×10^{-3} μM), rRac1 (0.1 μM), and rp67-phox (0.5 μM) in the presence or absence of rp47-phox (0.17 μM) and two concentrations of rp40-phox−GST (0.15 and 0.30 μM). Results are mean average (±SD) from three experiments.

First, there was no correlation between any of the two populations of deglycosylated cytochrome b_{558} and the control liposomes. The diameter of native cytochrome b_{558} liposomes (146 nm) was more than twice that of the deglycosylated hemoprotein (68 nm) (Table 1). The height of the liposomes was calculated from a software-derived cross section of the liposome at maximum diameter. The height of liposomes was 4−5 nm within error limits corresponding to a collapse of the structures, but without spreading to form a continuous bilayer. This is in agreement with the known effects of glycosylated lipids on rigidifying membranes, promoting the stability of large liposomes (*38*). Moreover, the results which show a difference in diameter between native and deglycosylated cytochrome b_{558} liposomes suggest different glycosylation states for the two types of cytochrome b_{558}, confirming results obtained by Western blotting (panels B and C of Figure 3, lanes 1).

The Limiting Cytosolic Factor in Oxidase Complex Assembly and Activation Is p67-phox. Cytochrome b_{558} purified from human neutrophils was used to investigate the assembly process through oxidase reconstitution in a cell-free assay. Native cytochrome b_{558} was incorporated into liposomes and incubated with rp67-phox added in a medium containing 0.1 μM rRac1, GTP[γ]S, $MgCl_2$, and optimal amounts of arachidonic acid. In a previous step, the optimum cytochrome b_{558} concentration had been determined similarly by the incubation of cytosol from healthy neutrophils with increasing amounts of cytochrome b_{558}; reconstituted oxidase activity was optimum at rates ranging between 100 and 150 mol of O_2^- s^{-1} (mol of heme b)$^{-1}$ for 2×10^{-3} μM cytochrome b_{558}. This latter concentration of purified cytochrome b_{558} was used in the cell-free assay illustrated in Figure 4A in which arachidonic acid-mediated oxidase reconstitution was induced by the sole addition of rp67-phox; a total reconstitution of oxidase activity was obtained at 1.5 μM rp67-phox added in the medium containing 0.1 μM rRac1. The further addition of 0.17 μM rp47-phox to the reconstitution medium increased the affinity of rp67-phox with cytochrome b_{558} as illustrated by a shift of the bell-shaped curve, giving an optimum oxidase activity similar to that obtained previously, for only 0.5 μM rp67-phox added to the medium. Moreover, the subsequent addition of rp40-phox−GST decreased the rate of oxidase turnover whether p47-phox was present or not, suggesting a competitive interaction of the factors during the in vitro reconstitution experiment (Figure 4B).

The direct involvement of p67-phox in the assembly process and the oxidase reconstitution was confirmed by complementation of p67-phox-deficient CGD EBV-B lymphocytes, the mutation of which had been previously identified (*30*). The cytosolic activating factors were collected from cytosols of either healthy or the latter CGD patients and isolated onto an Ig anti p47-phox affinity matrix (*15*). A complementation experiment was performed by incubating 2×10^{-3} μM cytochrome b_{558} purified from neutrophils with the cytosolic activating factors previously isolated; increasing

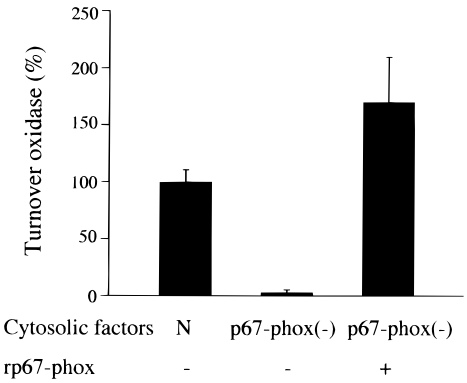

FIGURE 5: Reconstitution of oxidase activity with the cytosol of EBV-B lymphocytes from a p67-phox-deficient CGD patient (*30*) and complementation with recombinant p67-phox. Cell-free activation of NADPH oxidase was performed as described in Materials and Methods, using cytochrome b_{558} purified from neutrophils (2×10^{-3} μM) and cytosolic factors purified from EBV-B lymphocyte cytosol of healthy (N) or p67-phox-deficient CGD patients (10 μg), complemented in some cases with recombinant p67-phox (0.09 μM). Rates of O_2^- production are represented as a percentage of the rate obtained with cytosolic factors purified from EBV-B lymphocyte cytosol of healthy patients [105 mol of O_2^- s^{-1} (mol of heme b)$^{-1}$]. Results are mean averages ($\pm$SD) from at least three experiments.

concentrations of rp67-phox were added to the reconstitution medium containing 0.1 μM rRac1, GTPγS, $MgCl_2$, and an optimal amount of arachidonic acid as described in Materials and Methods. The results illustrated in Figure 5 demonstrated that a total restoration of oxidase activity versus control was obtained by the addition of 0.09 μM rp67-phox to the medium.

Atomic Force Microscopy Investigation of the Assembled Oxidase Complex. The changes in height of the liposomes during assembly of the oxidase complex were investigated by AFM. Purified cytochrome b_{558} either from neutrophils or from EBV-B lymphocytes was incorporated into liposomes and incubated with cytosolic factors added as recombinant proteins or in cytosol. The reconstitution medium contained, as previously described, rRac1, GTPγS, and $MgCl_2$. An optimal amount of arachidonic acid was added to initiate oxidase reconstitution and assembly. Then "activated" liposomes, that is, collected assembled complex, were allowed to adhere to a mica surface and washed with water before observation using AFM in air. Images of native cytochrome b_{558} liposomes and that after assembly with rp67-phox are shown in Figure 6 (left and right, respectively). The protrusion images have bell-shaped profiles, and the diameter of each was determined as described in Materials and Methods. The assembled complex demonstrated a high level of adhesion to mica. Apart from large protrusions, a number of small images are seen. According to the sizes, these protrusions can be divided into two groups depending on activated (assembled complex) or nonactivated liposomes (cytochrome b_{558} alone).

The model proposed for the assembly of the active complex is given in Figure 7. The height of the bilayer and that of cytochrome b_{558} in the collapsed liposomes are 2.5 nm as calculated from the height of the liposomes divided by 2; this arises from the collapse of the liposomes giving rise to two bilayers at the surface, compared to the value of 3−4 nm reported for erythrocyte membranes determined by

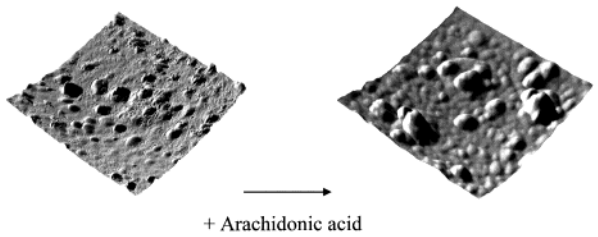

FIGURE 6: Topography of the NADPH oxidase complex after assembly. Imaging of cytochrome b_{558} liposomes before and after activation with arachidonic acid. Ten microliters of reconstituted oxidase activity medium (prepared as described in Materials and Methods) containing cytochrome b_{558} purified from neutrophils (2×10^{-3} μM) and neutrophil cytosol (300 μg) were collected before and after addition of arachidonic acid (60 nmol), spread on a mica surface, and observed by AFM.

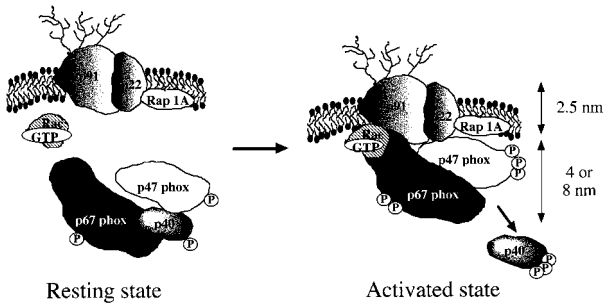

FIGURE 7: Representative model of the NADPH oxidase complex. In the resting state, cytosolic factors p47-phox, p67-phox, and p40-phox form a complex in the cytosol. After activation of oxidase, they translocate to the membrane where p67-phox and p47-phox associate with cytochrome b_{558}, forming a complex 4 or 8 nm high. P represents one or more phosphate groups.

surface plasmon resonance (*29*), or the value of 3.6 nm determined with X-ray diffraction (*39*). The lower value observed here may arise from the water contamination layer covering the surface from which the liposomes protrude. Some compression of the liposome structure may also occur, and thus, underestimation of the height values may exist; however, the difference will be less than 1 nm, as derived from the difference between the expected and observed values for the liposomes alone. However, the size of the assembled complex was determined by the difference from this value. Thus, the activated complex has a height of 4 or 8 nm, the two different values depending on whether the complex is presented as expected at both faces of the liposomes or only along one face. The first hypothesis seems most probable, and we thus propose that the cytosolic complex, containing p47-phox, p67-phox, and Rac1, has a height of 4 nm after oxidase activation and association with cytochrome b_{558}.

Correlation between Assembly and Activation of the Oxidase Complex through AFM and Cell-Free Assay Reconstitution Experiments. To investigate the limiting factors of oxidase assembly and activation, the effect of oxidase reconstitution was analyzed using AFM and by measuring oxidase turnover. Two reconstitution experiments were carried out; in the first type, reconstitution was mediated by incubating cytochrome b_{558} purified from neutrophils with either rp67-phox or rp47-phox in the presence (or not) of rp40-phox−GST (Table 3). The results illustrated in Table 3 demonstrate that rp67-phox alone is able to mediate assembly and activation; the size of the collected assembled

Table 2: Measurement of Liposome Size before and after Assembly of the Oxidase Complex[a]

	cytochrome b_{558} liposomes			
	neutrophils		EBV-B lymphocytes	
	before assembly	after assembly	before assembly	after assembly
diameter (nm)	147 ± 12	146 ± 8	164 ± 14	165 ± 22
height (nm)	5 ± 1	13 ± 1	4 ± 1	14 ± 2
n	25	21	25	28

[a] A 10 μL volume of reconstituted oxidase activity medium containing purified native cytochrome b_{558} from neutrophils or EBV-B lymphocytes (2×10^{-3} μM) and 300 μg of neutrophil cytosol (prepared as described in Materials and Methods) was collected before and after addition of arachidonic acid (60 nmol) and spread on a mica surface for observation by AFM. The diameter and height were calculated as described in the legend of Figure 1 (n = number of liposome images; results are means ± SD).

Table 3: Correlation of Assembly and Activation Steps of the Oxidase Complex[a]

system	liposome height (nm)		rate of oxidase turnover [mol of O_2^- s^{-1} mol of heme b)$^{-1}$]
	before activation	after activation	
Cyt b_{558} (PMN) + rRac1	5 ± 1	6 ± 2	20 ± 4
+ rp67-phox	5 ± 2	11 ± 2	95 ± 8
+ rp47-phox	4 ± 1	12 ± 3	14 ± 5
+ rp67-phox + rp40-phox-GST	10 ± 2	13 ± 3	35 ± 4
+ rp67-phox + rp47-phox + rp40-phox-GST	5 ± 2	12 ± 3	42 ± 3
+ rp47-phox + rp40-phox-GST	9 ± 2	9 ± 3	−

[a] Reconstituted oxidase activity medium was prepared as described in Materials and Methods, with cytochrome b_{558} purified from neutrophils (2×10^{-3} μM) and recombinant cytosolic factors: rRac1 (0.1 μM), rp67-phox (1.5 μM), and rp40-phox−GST (0.15 μM) in a final volume of 100 μL. In some experiments, rp47-phox (0.17 μM) was added to the medium; under these conditions, the p67-phox concentration was three times lower, which is 0.5 μM. Oxidase activation was obtained by addition of an optimal amount of arachidonic acid. Turnover was assessed by the ferricytochrome *c* reduction. The liposome size before and after assembly of oxidase complex was determined after AFM observation and measurement by using Topometrix software. Results are expressed as means ± SD.

complex is similar to that measured when the three factors, p67-phox, p47-phox, and p40-phox−GST, are present. Moreover, the reconstituted oxidase activity measured as turnover is in the same range as that obtained when cytochrome b_{558} is incubated with control neutrophil cytosol (Table 4). Contrary to these observations, the presence of the sole p47-phox in the reconstitution medium induces assembly but no activity.

The presence of p40-phox leads to two effects: first to a decrease in oxidase activity of the complex [35 mol of O_2^- s^{-1} (mol of heme b)$^{-1}$ vs 95 mol of O_2^- s^{-1} mol of heme b)$^{-1}$ for p67-phox], illustrating the inhibitory effect of the p40-phox factor on oxidase activity, and second in the presence of either p67-phox or p47-phox alone to a conformational change, even before activation (respective preactivation heights of 10 and 9 nm) (Table 3). When p40-phox, p47-phox, and p67-phox are present, this preactivation conformational change is absent (Table 3) and activation leads to an increase in liposome height (from 5 to 12 nm).

Table 4: NADPH Oxidase Assembly and Activation[a]

system	liposome height (nm)		rate of oxidase turnover [mol of O_2^- s^{-1} (mol of heme b)$^{-1}$]
	before activation	after activation	
Cyt. b_{558} (PMN) + neutrophil cytosol	5 ± 1	13 ± 1	89 ± 11
Cyt. b_{558} (PMN) + EBV-BL cytosol	5 ± 2	14 ± 3	50 ± 7
Cyt. b_{558} (PMN) + cytosol from p67-phox (−) EBV-BL	8 ± 3	11 ± 2	10 ± 3

[a] Reconstituted oxidase activity medium was prepared as described in Materials and Methods, with cytochrome b_{558} purified from neutrophils (2×10^{-3} μM) and cytosol from either neutrophils (300 μg) or EBV-B lymphocytes (EBV-BL) from control or p67-phox-deficient CGD patients (300 μg) in a final volume of 100 μL. Oxidase activation was obtained by addition of an optimal amount of arachidonic acid. Turnover of reconstituted oxidase was assessed by the ferricytochrome *c* reduction. The liposome size before and after assembly of the oxidase complex was determined after AFM observation and measurement by using Topometrix software. Results are expressd as means ± SD.

These observations were corroborated in a second type of reconstitution experiment where the cytosol of either healthy or p67-phox-deficient CGD EBV-B lymphocytes and that from control neutrophils were used instead of recombinant cytosolic factors (Table 4). The results demonstrate that the conformational change of cytochrome b_{558} is induced whatever cytosol type is used. They suggest that contrary to oxidase turnover it does not depend on the concentration of the factors which differs in neutrophils and EBV-B lymphocytes (*40*). When the cytosol of a p67-phox-deficient CGD patient is added in the reconstitution medium as expected, the liposome height increased but there was no reconstituted oxidase activity.

DISCUSSION

An atomic force microscope is a novel high-resolution instrument for the measurement and imaging of objects at the nanometer scale (*39*). One of its main benefits is the ability to investigate biological material in its native state, avoiding all processing such as fixation, dehydration embedding sectioning, and staining required in classical electron microscopy. The resolution of this precise method of the surface topography quantitation depends on both the relief of the sample and the geometry of the tip (*41*). Investigations were carried out in the noncontact mode where artifactual interactions between the tip and the sample are much less important than in the tapping mode because in theory, the tip is never in contact with the sample (*42*). We established an AFM imaging procedure that allowed us not only to visualize for the first time topography of cytochrome b_{558} incorporated into liposomes but also to analyze quantitatively the cytochrome b_{558} conformational change induced in the assembly of oxidase complex by the arachidonic acid. The results led us to propose a model of NADPH oxidase assembly where the cytosolic complex is 4 nm high. Immunoelectron microscopy had previously shown cytosolic oxidase components grouped in 3−10 nm clusters (*43*) at the membrane level after NADPH oxidase activation.

The successful application of AFM to the structural analysis of biological complexes opens the way to exploring

the structure−function relationships as shown for the oxidase complex in Tables 3 and 4. Atomic force microscopy investigation of NADPH oxidase assembly was correlated to oxidase turnover assessed at the molecular level. Whatever cytosolic factor involved in the binding with cytochrome b_{558} (p67-phox and/or p47-phox), the assembly process resulted in a change in cytochrome b_{558} conformation, but the critical factor of activation is p67-phox; in fact, the data presented here relative to cell-free oxidase reconstitution experiments and to p67-phox-deficient CGD complementation (ref *15* and this work) clearly suggest, as proposed by Lambeth (*18*, *44*), Pick (*19*), and Curnutte (*45*, *46*), that the role of p47-phox is to provide higher-affinity binding site(s) for the association of p67-phox and Rac1 or -2 with cytochrome b_{558}. Oxidase is latent at resting state; latency is favored by compartmentalization of the different components through membrane, cytoskeleton, and cytosol (*47*) as by the molecular association of p40-phox with p67-phox (*15*). During assembly, the cytosolic factors translocate to the membrane, and we propose that p67-phox has to dissociate from p40-phox to mediate optimum oxidase activation; Rac-GTP has been reported to be an effector of the dissociation (*17*). Moreover, Rac-GTP is assumed to participate in oxidase activation through its interaction with the N-terminal region of p67-phox (*48*). In vivo to obtain oxidase activity, both p47-phox and p67-phox have to bind with cytochrome b_{558} (*49*) and specific interaction sites have been identified on p22-phox and gp91-phox (*50*−*52*). We demonstrated also that both p47-phox and p67-phox are involved in the assembly process, but an interesting finding of this work is the dissociation of the assembly from the activation steps of oxidase complex. Contrary to that observed after addition of p67-phox alone which was shown to initiate both assembly and activation of NADPH oxidase, the binding of the sole p47-phox with cytochrome b_{558} allowed a similar structural conformational change of cytochrome b_{558} as shown through AFM, but the resultant complex exhibited no electron transfer activity.

The amphiphilic arachidonic acid reagent necessary for in vitro activation was recently shown to interact with p47-phox (*53*) and also to increase the affinity of the oxidase for oxygen through cytochrome b_{558} (*54*). Regulation mechanisms of NADPH oxidase activity involve both catalytic and regulator components; the stable conformation of cytochrome b_{558} needs p22-phox and gp91-phox, but the latter membrane factor mediates catalysis. In the oxidase assembly, we demonstrated that p67-phox is the sole factor that is able to initiate the electron transfer and that p47-phox could proceed as a positive regulator enhancing oxidase activation, suggesting, as recently reported (*44*), two different levels of oxidase activation states.

The results argue in favor of allosteric regulation mechanisms of the phagocyte oxidase complex in which gp91-phox and p67-phox could be directly or not involved in catalysis, the positive regulation of which being mediated through the binding of p47-phox with cytochrome b_{558}; however, the oligomeric structure of the oxidase machinery is as yet unresolved. Atomic force microscopy was able to distinguish two cytochrome b_{558} conformational states, which are required during the transition from the inactive to the active state of the assembled oxidase complex. More work is necessary to correlate inactivation of NADPH oxidase to dissassembly of the complex as recently suggested (*55*).

REFERENCES

1. Morel, F., Doussière, J., and Vignais, P. V. (1991) *Eur. J. Biochem. 201*, 523−546.
2. Segal, A. W., and Abo, A. (1993) *Trends Biochem. Sci. 18*, 43−47.
3. Huang, J., Hitt, N. D., and Kleinberg, M. E. (1995) *Biochemistry 34*, 16753−16757.
4. Harper, A. M., Chaplin, M. F., and Segal, A. W. (1985) *Biochem. J. 227*, 783−788.
5. Parkos, C. A., Allen, R. A., Cochrane, C. G., and Jesaitis, A. J. (1987) *J. Clin. Invest. 80*, 732−742.
6. Wallach, T. M., and Segal, A. W. (1997) *Biochem. J. 321*, 583−585.
7. Yu, L., Quinn, M. T., Cross, A. R., and Dinauer, M. C. (1998) *Proc. Natl. Acad. Sci. U.S.A. 95*, 7993−7998.
8. Yu, L., Zhen, L., and Dinauer, M. C. (1997) *J. Biol. Chem. 272*, 27288−27294.
9. Wientjes, F. B., Panayotou, G., Reeves, E., and Segal, A. W. (1996) *Biochem. J. 317*, 919−924.
10. Kreck, M. L., Freeman, J. L., Abo, A., and Lambeth, J. D. (1996) *Biochemistry 35*, 15683−15692.
11. Sathyamoorthy, M., de Mendez, I., Adams, A. G., and Leto, T. L. (1997) *J. Biol. Chem. 272*, 9141−9146.
12. El Benna, J., Dang, P. M. C., Gandry, M., Fay, M., Morel, F., Hakim, J., and Gougerot-Pocidalo, M. A. (1997) *J. Biol. Chem. 272*, 17204−17208.
13. Bouin, A. P., Grandvaux, N., Vignais, P. V., and Fuchs, A. (1998) *J. Biol. Chem. 273*, 30097−30103.
14. Dang, P. M. C., Babior, B. M., and Smith, R. M. (1999) *Biochemistry 38*, 5746−5753.
15. Vergnaud, S., Paclet, M. H., El Benna, J., Pocidalo, M. A., and Morel, F. (2000) *Eur. J. Biochem. 267*, 1059−1067.
16. Dieckmann, D., Abo, A., Johnston, C., Segal, A. W., and Hall, A. (1994) *Science 265*, 531−533.
17. Rinkel, L. A., Faris, S. L., Hitt, N. D., and Kleinberg, M. E. (1999) *Biochem. Biophys. Res. Commun. 263*, 118−122.
18. Freeman, J. L., and Lambeth, J. D. (1996) *J. Biol. Chem. 271*, 22578−22582.
19. Koshkin, V., Lotan, O., and Pick, E. (1996) *J. Biol. Chem. 271*, 30326−30329.
20. Cohen-Tanugi, L., Morel, F., Pilloud-Dagher, M. C., Seigneurin, J. M., François, P., Bost, M., and Vignais, P. V. (1991) *Eur. J. Biochem. 202*, 649−655.
21. Knoller, S., Shpungin, S., and Pick, E. (1991) *J. Biol. Chem. 266*, 2795−2804.
22. Neff, D., Tripathi, S., Middendorf, K., Butt, H. J., Bamberg, E., and Dencher, N. A. (1997) *J. Struct. Biol. 119*, 139−148.
23. Wiesendanger, R. (1994) *Scanning Probe Microscopy and Spectroscopy, Methods and Applications*, Cambridge University Press, Cambridge, U.K.
24. Colton, R. J., Ed. (1998) *Procedures in Scanning Probe Microscopies*, Wiley, Winchester, U.K.
25. Muller, D. J., Amrein, M., and Engel, A. (1997) *J. Struct. Biol. 119*, 172−188.
26. Engel, A., Lyubchenko, Y., and Muller, D. (1999) *Trends Cell Biol. 9*, 77−80.
27. Allen, S., Chen, X., Davies, J., Davies, M. C., Dawkes, A. C., Edwards, J. C., Roberts, C. J., Sefton, J., Tendler, S. J. B., and Williams, P. M. (1997) *Biochemistry 36*, 7457−7463.
28. Kirpotin, D., Hong, K., Mullah, N., Papahadjopoulos, D., and Zalipsky, S. (1996) *FEBS Lett. 388*, 115−118.
29. Rao, N. M., Plant, A. L., Silin, V., Wight, S., and Hui, S. W. (1997) *Biophys. J. 73*, 3066−3077.
30. Cohen Tanugi-Cholley, L., Issartel, J. P., Lunardi, J., Freycon, F., Morel, F., and Vignais, P. V. (1995) *Blood 85*, 242−249.
31. Batot, G., Martel, C., Capdeville, N., Wientjes, F., and Morel, F. (1995) *Eur. J. Biochem. 234*, 208−215.
32. Abo, A., Boyhan, A., West, I., Thrasher, A. J., and Segal, A. W. (1992) *J. Biol. Chem. 267*, 16767−16770.
33. Fuchs, A., Bouin, A. P., Rabilloud, T., and Vignais, P. V. (1997) *Eur. J. Biochem. 249*, 531−539.

34. Batot, G., Paclet, M. H., Doussière, J., Vergnaud, S., Martel, C., Vignais, P. V., and Morel, F. (1998) *Biochim. Biophys. Acta 1406*, 188−202.
35. Laemmli, U. K. (1970) *Nature 227*, 680−685.
36. Wray, W., Boulikas, T., Wray, V., and Hancock, R. (1981) *Anal. Biochem. 118*, 197−203.
37. Towbin, H., Staehelin, T., and Gordon, J. (1979) *Proc. Natl. Acad. Sci. U.S.A. 76*, 4350−4354.
38. Lasic, D. D. (1998) *Trends Biotechnol. 16*, 307−321.
39. Warren, R. C. (1987) in *Physics and the Architecture of Cell Membranes* (Hilger, A., Ed.) pp 81−95, Bristol, U.K.
40. Kobayashi, S., Imajoh-Ohmi, S., Kuribayashi, F., Nunoi, H., Nakamura, M., and Kanegasaki, S. (1995) *J. Biochem. 117*, 758−765.
41. Bustamante, C., Vesenka, J., Tang, C. L., Lees, W., Guthold, M., and Keller, R. (1992) *Biochemistry 31*, 22−26.
42. Hanssen, E., Franc, S., and Garrone, R. (1998) *Biol. Cell 90*, 223−228.
43. Wientjes, F. B., Segal, A. W., and Hartwig, J. H. (1997) *J. Leukocyte Biol. 61*, 303−312.
44. Nisimoto, Y., Motalebi, S., Han, C. H., and Lambeth, D. (1999) *J. Biol. Chem. 274*, 22999−23005.
45. Cross, A. R., and Curnutte, J. T. (1995) *J. Biol. Chem. 270*, 6543−6548.
46. Cross, A. R., Erickson, R. W., and Curnutte, J. T. (1999) *Biochem. J. 341*, 251−255.
47. El Benna, J., Dang, P. M. C., Andrieu, V., Vergnaud, S., Dewas, C., Cachia, O., Fay, M., Morel, F., Cholley-Martin, S., Hakim, J., and Gougerot-Pocidalo, M. A. (1999) *J. Leukocyte Biol. 66*, 1−7.
48. Koga, M., Terasawa, H., Nunoi, H., Takestrige, K., Inagaki, F., and Sumimoto, H. (1999) *J. Biol. Chem. 274*, 25051−25060.
49. Heyworth, P. G., Curnutte, J. T., Nauseef, W. M., Volpp, B. D., Pearson, D. W., Rosen, H., and Clark, R. A. (1991) *J. Clin. Invest. 87*, 352−356.
50. De Leo, F. R., Nauseef, W. M., Jesaitis, A. J., Burritt, J. B., Clark, R. A., and Quinn, M. T. (1995) *J. Biol. Chem. 270*, 26246−26251.
51. De Mendez, I., Homayounpour, N., and Leto, L. (1997) *Mol. Cell. Biol. 17*, 2177−2185.
52. Han, C. H., Freeman, J. L. R., Lee, J., Motalebi, S. A., and Lambeth, J. D. (1998) *J. Biol. Chem. 273*, 16663−16668.
53. Sumimoto, H., Kage, Y., Nunoi, H., Sasaki, H., Nose, T., Fukumaki, Y., Ohno, M., Minakami, S., and Takeshige, K. (1994) *Proc. Natl. Acad. Sci. U.S.A. 91*, 5345−5349.
54. Doussière, J., Bouzidi, F., Poinas, A., Gaillard, J., and Vignais, P. V. (1999) *Biochemistry 38*, 16394−16406.
55. De Leo, F. R., Allen, L. A. H., Apicella, M., and Nauseef, W. M. (1999) *J. Immunol. 163*, 6732−6740.

BI000483J